A Smart High Accuracy Calibration Algorithm for 3-D Piezoresistive Stress Sensor

Mohammed O. Kayed, Amr A. Balbola, and Walied A. Moussa

***Abstract*— Numerical and experimental sensitivity analyses in this paper indicate that the accuracy of a silicon multi-element piezoresistive (PR) stress sensor can be dramatically influenced by the microfabrication non-uniformity and the uncertainties in the values of the PR coefficients and the thermal coefficient of resistance (TCR). The results showed that errors as large as 70% FS or more, in the extracted stress values, may be obtained due to uncertainty of about 2.5% in the values of PR coefficients. This paper aims to evaluate the capabilities of the artificial neural network (ANN) to eliminate the error in stress measurement, due to the fabrication non-uniformity within wafer, wafer-to-wafer, and batch-to-batch, for multi-element PR sensing rosettes. In this paper, sensing chips from two different batches were integrated in building the ANN and testing its performance. The proposed calibration technique employs the neural network fitting Toolbox in MATLAB to generate a two-layer feed-forward network, with sigmoid hidden neurons and linear output neurons. Three different configurations of calibration were designed to test the generalization abilities of the ANN in capturing the in-plane stress components exerted on the silicon chip. The results showed that ANN is capable of accurately predicting the stresses applied to the sensing chip with maximum stress error of 1.5% FS with no need for individual, expensive, and time-consuming calibration process for each sensor.**

***Index Terms*— Calibration, neural networks, n-type silicon, stress sensor, piezoresistivity, piezoresistive device, silicon sensor.**

I. Introduction

MONITORING the full mechanical stress and strain fields within a certain material is essential to determine the structural integrity and define a failure threshold for such material. The piezoresistive sensors are commonly used in such stress-sensing applications, since they offer a direct linear relationship with applied stresses. In particular, the doped silicon stress sensors exhibit exceptional piezoresistive behavior, because of their low cost, small size, good linearity, low power consumption, batch fabrication capability and absence of hysteresis [1]. Moreover, the unique properties of the crystalline silicon can be utilized to develop a piezoresistive three-dimensional (3D) stress sensor that is capable of measuring the all six stress components. Extraction of these stress components is pivotal in applications in which both in-plane and out-of-plane stresses have to be monitored like in electronic packaging or general composite structures. In such applications, it is essential to determine the stresses exerted on the surface of the structures and stresses responsible for delamination.

The development of a piezoresistive stress sensor that is capable of measuring the 3D stress components was early carried out by a group of researchers at Auburn University [2], [3]. Through using a rosette of dual polarity elements, they could form a set of independent linear equations to solve for the 3D stress components. The authors' group found that a single polarity (n-type) silicon rosette made up of ten elements can be utilized to extract the all six stress components with temperature compensation [4], [5]. This is because of the fact that the shear piezoresistive (PR) coefficient π_{44}, for n-type silicon, is independent of impurity concentration unlike the other PR coefficients, π_{11} and π_{12}.

Previous efforts were conducted to analyze the sources of error accompanying stress measurements using piezoresistive sensors. Jaeger *et al.* [6], [7] studied the errors associated with the calibration of the piezoresistive stress sensors. Their results indicate that uncertainties of 10% or more in PR coefficients' values might be obtained from experimental calibration of the (100) stress sensors, which in turn could produce large errors in extracted stress values. Error analysis was conducted to study the effect of measurement and calibration errors on the output of the (111) stress sensors by Hussain *et al.* [8]. They concluded that the sensitivity is dependent on the stress distribution over the surface of the sensing chip. Their findings also confirmed the utilization of temperature compensated rosette configurations, since they are less sensitive to measurement uncertainty. Cho *et al.* [9] investigated the temperature effects on the PR coefficients and TCR in the stress sensors. It was found that the PR coefficients linearly decrease in magnitude for both n-type and p-type materials with the increase in operating temperature.

Some researchers proposed novel designs and some fabrication processes as compensation systems to overcome the sources of error associated with the measurement and thus enhance the accuracy of sensors [10]–[12]. But, other smart compensation approaches have been provided using signal-conditioning interfaces, hardware-based and software-based, for thermal drifts and nonlinearity issues in piezoresistive sensors [13], [14]. For software-based smart calibration systems, the ANNs provide an efficient tool for sensor compensation and linearity correction [15]. The ANNs were successfully

Manuscript received November 28, 2016; accepted December 24, 2016. Date of publication December 28, 2016; date of current version February 7, 2017. This work was supported in part by the Canadian Microsystems Corporation and in part by the Natural Sciences and Engineering Research Council of Canada. The associate editor coordinating the review of this paper and approving it for publication was Prof. Weileun Fang.

M. O. Kayed and A. A. Balbola are with the Mechanical Engineering Department, University of Alberta, Edmonton, AB T6G 2G8, Canada, and also with the Faculty of Engineering, Cairo University, Giza 12613, Egypt (e-mail: mkayed@ualberta.ca; mkayed@eng.cu.edu.eg; amr.balbola@ualberta.ca; amr.balbola@cu.edu.eg).

W. A. Moussa is with the Mechanical Engineering Department, University of Alberta, Edmonton, AB T6G 2G8, Canada (e-mail: walied.moussa@ualberta.ca).

Digital Object Identifier 10.1109/JSEN.2016.2645701

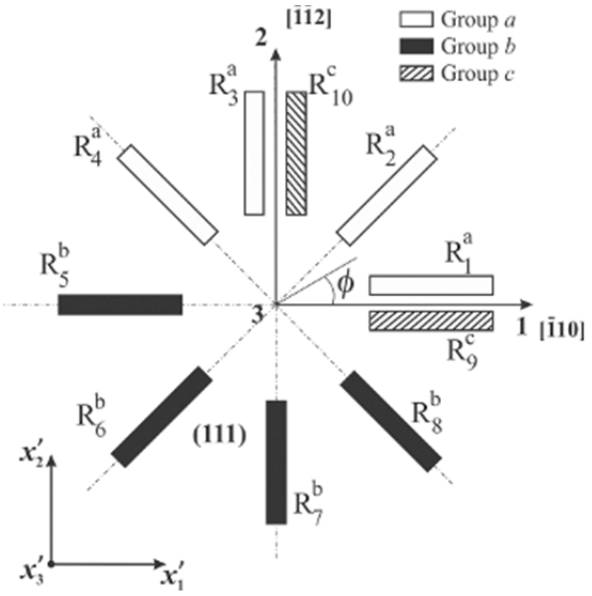

Fig. 1. Ten-element piezoresistive sensing rosette [4].

utilized as an inverse modeling method for mapping nonlinear input-output relations of sensor signals [16]–[20].

In this Paper, numerical and experimental sensitivity analyses of a single-polarity 3D piezoresistive stress sensor, which was devised by the authors' group [5], are conducted to study the effect of fabrication non-uniformity within wafer, wafer-to-wafer and batch-to-batch on the values of PR coefficients and TCR and the sensor's accuracy as well. This paper also proposes a new calibration algorithm, using ANNs, to improve the 3D stress sensor's performance by eliminating the measurement error due to the uncertainties in the values of PR coefficients and TCR obtained from conventional experimental calibration techniques. This proposed calibration algorithm abolishes the need for a costly and time consuming calibration process for each sensor in a fabricated batch.

II. Single-Polarity 3D Piezoresistive Stress Sensor

A. Theory

The theory of the ten-element sensing rosette employed in this work has been previously presented by the authors' group in earlier publications [4], [5]. Fig. 1 shows a schematic of the ten-element rosette with the piezoresistors oriented over the (111) silicon plane with 45 degrees increments. In this work, the authors only focus on examining the sensor's accuracy while extracting the in-plane stress components σ_{11}, σ_{12} and σ_{22}. So, this section will only present the equations of in-plane stress components, equations 1-3, in their final form. Where, σ'_{ij} is the stress components given in the chip coordinate system x'_i (i = 1−3), as indicated in Fig. 1. While, B_i (i =1,2,3) are functions of the PR coefficients π_{11}, π_{12}, and π_{44}. Whereas, α denotes the first order TCR. Superscripts a, b, and c indicate three groups of elements with different impurity concentration and PR coefficients and TCR while the subscripts 1 to 10 on $\Delta R/R$ indicate the number of the sensing element.

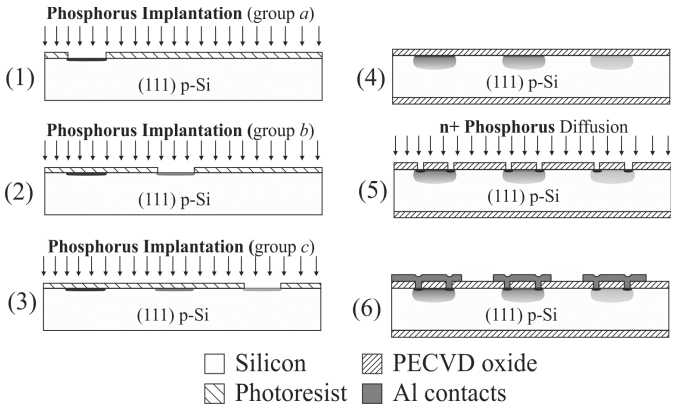

Fig. 2. Microfabrication process flow of the sensing chip [21].

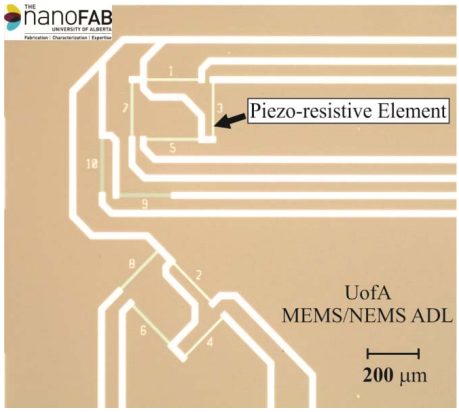

Fig. 3. The fabricated ten-element sensing rosette.

TABLE I
Experimental Impurity Peak Concentrations (cm^{-3})

Group *a*	$7.4x10^{19}$
Group *b*	$4.7x10^{19}$
Group c	$2.9x10^{19}$

B. Microfabrication

A three-step phosphorus ion implantation process was carried out at Innovion Inc. to obtain three groups of piezoresistors, a, b and c with three different surface concentrations. Ion implantation doses were $1.7 \times 10^{15}cm^{-2}$, $1.1 \times 10^{15}cm^{-2}$, and $7.5 \times 10^{14}cm^{-2}$ for groups, a, b, and c, respectively, and the implantation energy was 80 keV. Fig. 2 and Fig. 3 show the microfabrication process flow of stress sensor and the fabricated ten-element sensing rosette, respectively. Two different batches of the sensing chip were fabricated in the micro and nanofabrication facility (nanoFAB) and the MEMS/NEMS Advanced Design Laboratory (ADL) at the University of Alberta.

The impurity concentration profile of each group was experimentally characterized by spreading resistance profiling (SRP) measurements at Solecon Laboratories Inc. The resulting peak concentrations of groups, a, b, and c are given in Table 1.

C. Calibration

In order to employ such multi-element sensing rosette in stress measurement, accurate values for the PR coefficients and TCR must be obtained. A detailed and careful experimental calibration procedure of the sensor has been presented by the authors' group in earlier publications [21], [22]. In this study, the authors followed the same procedure to calibrate B_1, B_2, B_3 and α, of groups, a, b and c, to correctly capture the in-plane stress components, as denoted in equations (1) to (3), as shown at bottom of this page. The calibration of B_1 and B_2 is carried out using a four-point bending setup, to apply a known uniaxial stress to a silicon beam with calibration resistors which are identical to the measurement elements, while B_3 is calibrated by applying a known hydrostatic pressure. Lastly, α is calibrated by applying a stress-free temperature load using an environmental chamber to control the thermal load. The average calibrated values of PR coefficients and TCR for 8 calibration elements are given in Table 2 with standard deviations noted between parentheses.

TABLE II
EXPERIMENTAL NOMINAL VALUES FOR B_i AND α^*

Group	a	b	c
B_1, TPa^{-1}	-153.74	-162.18	-170.66
	(3.68)	(3.14)	(3.18)
B_2, TPa^{-1}	116.13	125.16	132.67
	(5.09)	(5.13)	(4.92)
B_3, TPa^{-1}	-37.5	-0.47	2.07
α, ppm/°C	1780.57	1526.63	1222.98
	(43.02)	(53.56)	(48.78)

* values between parenthesis are standard deviations

III. SENSITIVITY ANALYSIS

In this section, the sensitivity of the in-plane stress components to the changes in values of the PR coefficients is investigated for the ten-element rosette. The sensitivity of stress component σ_{ij} to changes in a given parameter P can be expressed as follows:

$$S_P^{\sigma_{ij}} = \frac{P}{\sigma_{ij}}\frac{\partial \sigma_{ij}}{\partial P} = \left(\frac{\partial \sigma_{ij}}{\sigma_{ij}}\right) \Big/ \left(\frac{\partial P}{P}\right) \tag{7}$$

Where, $S_P^{\sigma_{ij}}$ is a dimensionless quantity that represents the ratio of the fractional change in stress that arises from a fractional change in the given parameter. For multi-element piezoresistive sensor, the interrelation between stress and PR coefficients variation is hard to analytically interpret. For instance, the sensitivity expression of σ_{11} to B_1^b variation for the ten-element sensor rosette is given in equation 8.

$$S_{B_1^b}^{\sigma_{11}} = \frac{B_1^b(B_3^a\alpha^c - B_3^c\alpha^a)}{2D_2}\left(\frac{\sigma_{22}}{\sigma_{11}} - 1\right) - \frac{B_1^b(B_2^a - B_3^a)}{2D_1}\left(\frac{\sigma_{22}}{\sigma_{11}} + 1\right) \tag{8}$$

It is clear that a higher complexity of interaction between PRCs is found. Therefore, the sensitivities have been investigated through numerical evaluation first, which is followed by an experimental verification phase in this section.

A. Numerical Analysis

To study the stress measurement error, due to fabrication non-uniformity and the uncertainties in the values of PR coefficients and TCR, random data sets of PR coefficients and TCR have been generated for the three groups a, b and c of

$$\sigma'_{11} = \frac{1}{2D_2}\left[\left(B_3^c\alpha^b - B_3^b\alpha^c\right)\left(\frac{\Delta R_1}{R_1} + \frac{\Delta R_3}{R_3}\right) + \left(B_3^a\alpha^c - B_3^c\alpha^a\right)\left(\frac{\Delta R_5}{R_5} + \frac{\Delta R_7}{R_7}\right) + \left(B_3^b\alpha^a - B_3^a\alpha^b\right)\left(\frac{\Delta R_9}{R_9} + \frac{\Delta R_{10}}{R_{10}}\right)\right] + \frac{1}{2D_1}\left[\left(B_2^b - B_3^b\right)\left(\frac{\Delta R_1}{R_1} - \frac{\Delta R_3}{R_3}\right) - \left(B_2^a - B_3^a\right)\left(\frac{\Delta R_5}{R_5} - \frac{\Delta R_7}{R_7}\right)\right] \tag{1}$$

$$\sigma'_{22} = \frac{1}{2D_2}\left[\left(B_3^c\alpha^b - B_3^b\alpha^c\right)\left(\frac{\Delta R_1}{R_1} + \frac{\Delta R_3}{R_3}\right) + \left(B_3^a\alpha^c - B_3^c\alpha^a\right)\left(\frac{\Delta R_5}{R_5} + \frac{\Delta R_7}{R_7}\right) + \left(B_3^b\alpha^a - B_3^a\alpha^b\right)\left(\frac{\Delta R_9}{R_9} + \frac{\Delta R_{10}}{R_{10}}\right)\right] - \frac{1}{2D_1}\left[\left(B_2^b - B_3^b\right)\left(\frac{\Delta R_1}{R_1} - \frac{\Delta R_3}{R_3}\right) - \left(B_2^a - B_3^a\right)\left(\frac{\Delta R_5}{R_5} - \frac{\Delta R_7}{R_7}\right)\right] \tag{2}$$

$$\sigma'_{12} = \frac{1}{D_1}\left[\frac{\left(B_2^b - B_3^b\right)}{2}\left(\frac{\Delta R_2}{R_2} - \frac{\Delta R_4}{R_4}\right) - \frac{\left(B_2^a - B_3^a\right)}{2}\left(\frac{\Delta R_6}{R_6} - \frac{\Delta R_8}{R_8}\right)\right] \tag{3}$$

Where,

$$B_1 = \frac{\pi_{11} + \pi_{12} + \pi_{44}}{2},\ B_2 = \frac{\pi_{11} + 5\pi_{12} - \pi_{44}}{6},\ \text{and} B_3 = \frac{\pi_{11} + 2\pi_{12} - \pi_{44}}{3} \tag{4}$$

And D_1 and D_2 are given by:

$$D_1 = B_1^a\left(B_2^b - B_3^b\right) + B_2^a\left(B_3^b - B_1^b\right) + B_3^a\left(B_1^b - B_2^b\right) \tag{5}$$

$$D_2 = B_3^a\left[(B_1^b + B_2^b)\alpha^c - (B_1^c + B_2^c)\alpha^b\right] + B_3^b\left[(B_1^c + B_2^c)\alpha^a - (B_1^a + B_2^a)\alpha^c\right] + B_3^c\left[(B_1^a + B_2^a)\alpha^b - (B_1^b + B_2^b)\alpha^a\right] \tag{6}$$

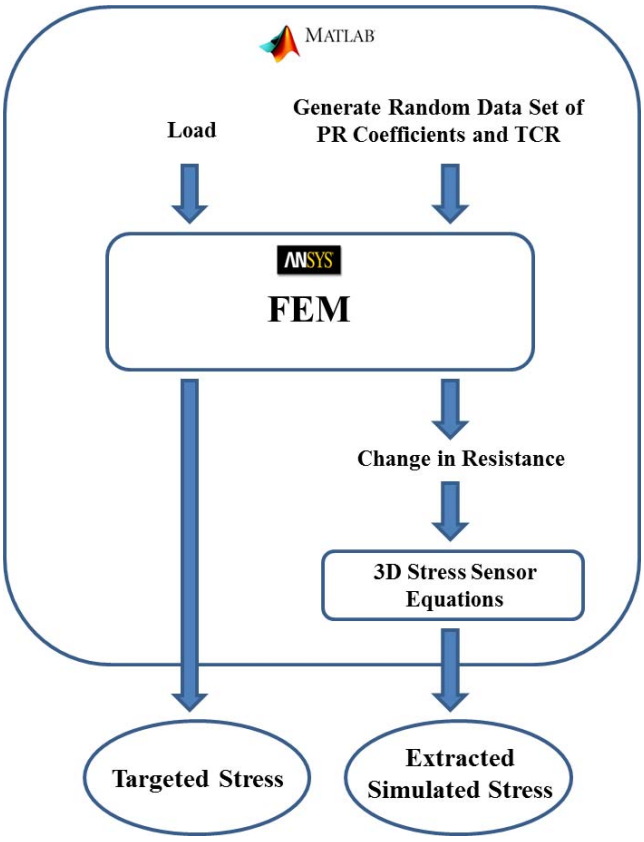

Fig. 4. Numerical sensitivity analysis flow diagram.

the sensing elements with relative standard deviation (RSD) of 2.5%. The mean values of these random data sets have been chosen equal to those obtained from the experimental calibration of the sensing chip, as given in Table 2.

Fig. 4 shows the flow diagram of the numerical sensitivity analysis utilized to investigate the effect of fabrication non-uniformity and the uncertainty in PR coefficients and TCR values on the sensor's capability to extract the in-plane stress components σ_{11}, σ_{12} and σ_{22}.

A finite element model (FEM) of the 3D stress sensing chip bonded to a PCB beam (FR-4) under four-point bending was developed using ANSYS®Multiphysics to calculate the average stress values exerted on the chip surface and the corresponding change in resistance of the ten sensing elements at the center rosette.

In FEM, three different cases S0, S45 and S90 were simulated, where the chip's axial-direction, x_1', is oriented to the beam's axial-direction, x_1, at 0, 45, and 90 degrees. These three cases S0, S45 and S90 were used to induce the in-plane stress components σ_{11}, σ_{12} and σ_{22}, respectively, at the center sensing rosette using four-point bending loading.

Fig. 5 to Fig. 7 show the deviation occurs while extracting the in-plane stress components due to a random variation in the PR coefficients' values with 2.5% RSD from the nominal value.

Targeted values are the simulated stresses exerted on the sensing chip and obtained from FEM. While Output values are the stresses extracted from equations 1-3 using the simulated change in resistance ($\Delta R/R$) obtained from FEM and

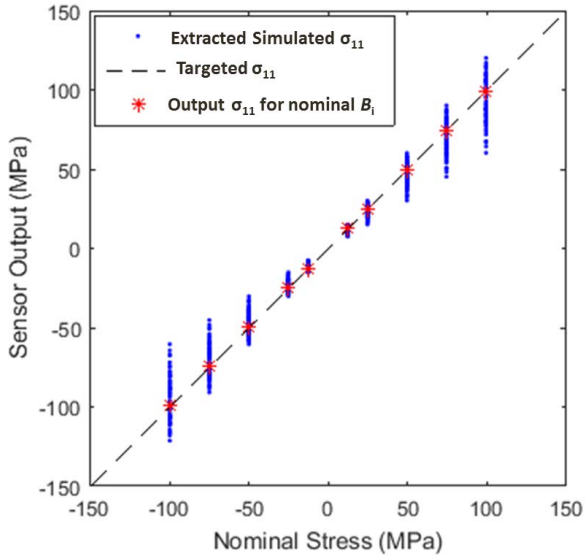

Fig. 5. Simulated stress error in σ_{11} for case S0.

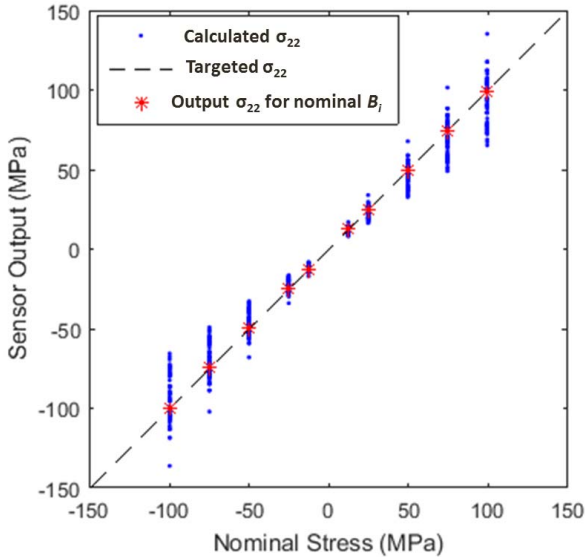

Fig. 6. Simulated stress error in σ_{22} for case S90.

nominal B_i values. The results show an excellent agreement between the FEM and the theory of the ten-element sensor for the same PR coefficients. As shown in Fig. 5 to Fig. 7, the fabrication non-uniformity and the uncertainties in PR coefficients may lead to large errors in extracted stress values. As in case S0, stress error of ~39% has been obtained while calculating σ_{11} produced on the sensing chip surface. It has also been noticed that σ_{12} is less sensitive to the deviation in PR coefficients and TCR values than both stress components σ_{11} and σ_{22}. This less sensitivity behavior of σ_{12} is attributed to its reduced equation form (equation 3) compared to the other stress components σ_{11} and σ_{22} (equations 1 and 2). As only 4 piezoresistors, R_2, R_4, R_6 and R_8, are used to extract σ_{12}. While extracting σ_{11} and σ_{22} need 6 piezoresistors, R_1, R_3, R_5, R_7, R_9 and R_{10}.

B. Experimental Analysis

An experimental sensitivity study was also conducted to investigate to what extent the errors in measuring the PR

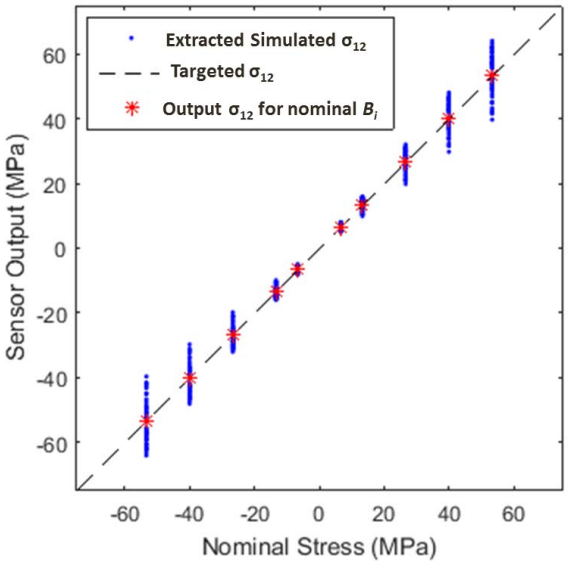

Fig. 7. Simulated stress error in σ_{12} for case S45.

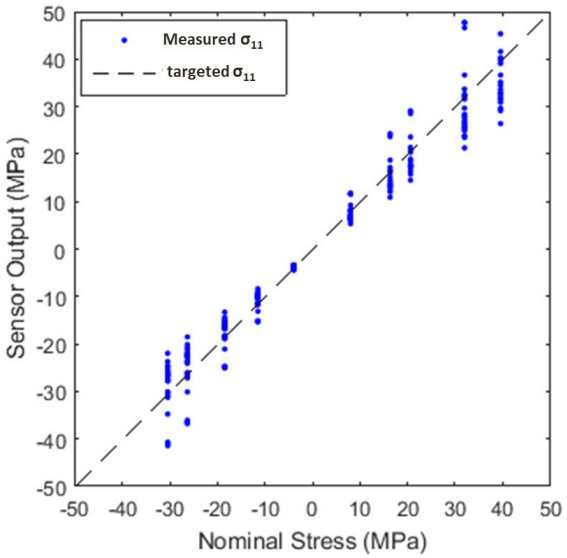

Fig. 8. Experimental stress error in σ_{11} for case S0.

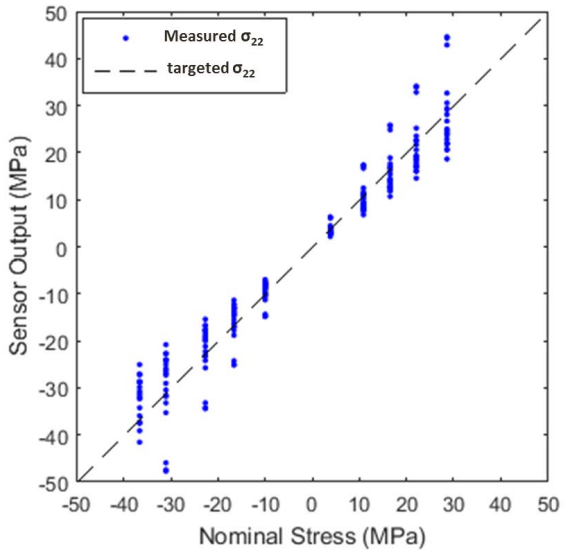

Fig. 9. Experimental stress error in σ_{22} for case S90.

coefficients can influence the accuracy of the ten-element 3D stress sensor. In Table 2, RSD of ∼2.5% was obtained during the calibration of PR coefficients of groups, a, b and c. To test the effect of PR coefficients' variation, due to fabrication non-uniformity, on the sensor's output, a random data set of PR coefficients of groups, a, b and c was constructed by using the experimental mean values and standard deviations.

Like the numerical sensitivity analysis, the sensing chip was attached to a PCB beam with three different orientations S0, S45 and S90 to induce the in-plane stress components σ_{11}, σ_{12} and σ_{22}, respectively, at the ten-element sensing rosette. The beam was subjected to 10 different loads that produce 10 corresponding average uniaxial stress within a range from −40 to 40 MPa on the sensing chip surface. For each load, the corresponding change in resistance (Δ *R/R*) of the ten-element center rosette was measured using the four-point bending testing setup, which is described in the next section.

For each output of the ten-element rosette, that represents a certain stress state at the center of the sensing chip's surface, the in-plane stress components were extracted from equations 1-3 using the PR coefficients experimental data set. These extracted stresses were compared to the targeted stresses exerted on the sensing chip. The targeted stress was estimated first using FEM, then the FEM was validated using a calibrated sensor. The FEM calculation results showed an excellent agreement (error less than 1.4%) with the results obtained from the calibrated sensor. Then, stress error due to the variation in PR coefficients, were evaluated.

Fig. 8 to Fig. 10 show the variation in stress measurements obtained while extracting the in-plane stress components σ_{11}, σ_{12} and σ_{22} exerted on the sensor's surface for cases S0, S45 and S90, respectively. It can be clearly seen that, the fabrication non-uniformity and the uncertainties in PR coefficients may lead to large errors in extracted stress values. As shown in Fig. 11, a stress error as large as 50% *FS* and 70% *FS* while extracting σ_{11} and σ_{22}, respectively, has been obtained due to 2.5 % RSD in the values of PR coefficients. As confirmed numerically, the results of experimental analysis also show that the ten-element sensing rosette is less sensitive to the variation in PR coefficients while extracting σ_{12} compared to the other in-plane stress components σ_{11} and σ_{22}.

IV. Neural Networks Calibration Algorithm

Both numerical and experimental sensitivity analyses, discussed in previous sections, indicate that the accuracy of the 3D piezoresistive stress sensor to extract the stress components is greatly affected by the uncertainties in the values of the PR coefficients due to fabrication non-uniformity. The ANNs can be used to build a smart calibration system that would be able to compensate all errors arise during fabrication and

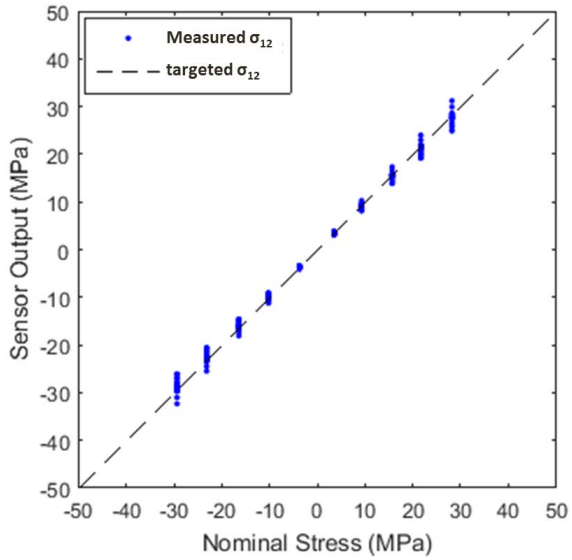

Fig. 10. Experimental stress error in σ_{12} for case S45.

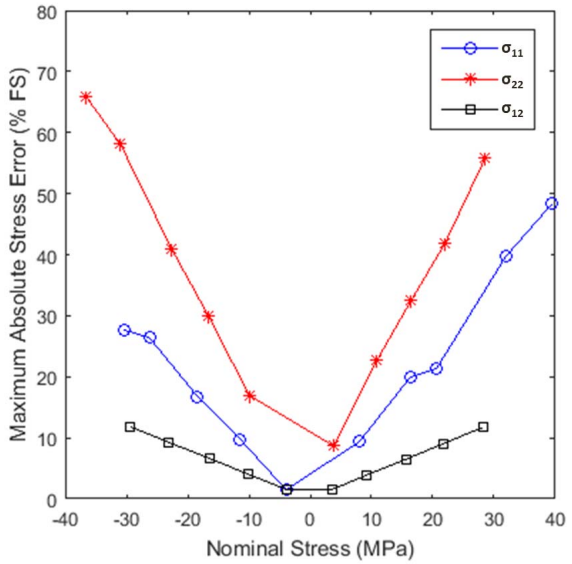

Fig. 11. Stress measurement error of 3D stress senor.

calibration that may lead to uncertainty in knowing the exact values of the PR coefficients. To consider the non-uniformity within the wafer, the sensing chips used in building and testing ANNs were selected from different locations across the wafer, specifically, around the periphery of the wafer and the middle of the wafer where the maximum non-uniformity within the wafer appears, [23]. In addition, to consider the non-uniformity from wafer-to-wafer or batch-to batch, sensing chips from different wafers of two different batches were utilized to evaluate the calibration capabilities of ANNs.

A. Testing Setup

To measure the resistance change of the ten sensing elements and the corresponding applied load on the beam at each loading increment, the testing setup, shown in Fig. 12, was used. The resistance measurement of each sensing element was carried out through supplying a constant current of 100 μA using a source meter and measuring the differential voltage change for each sensing element using a 6½digit multi-meter. The switching between the sensing elements was carried out manually using a rotary switch. An incremental load (F), from 0 to around 7.5 N, with 1.5 N step, was applied to the PCB beam. For each load, the corresponding average stresses, exerted at the center of the sensing chip, were estimated using FEM.

B. Software Setup

Neural Network Fitting Toolbox in Matlab was used to generate a two-layer feed-forward network, with sigmoid hidden neurons and linear output neurons, that is capable of predicting the stresses applied on the sensing chip with minimum stress error. Below are the specific steps of creating neural network calibration algorithm:

- Collect data (i.e. the changes in resistance ($\Delta R/R$) of the sensing elements, which are the ANN inputs, and the corresponding stresses, which are the ANN targets).
- Randomly divide the collected data into training data and testing data with ratio of 3 to 2.
- Configure the network.
- Train the network using training data.
- Validate the network using testing data.
- Perform some analysis of the network response during training, validation and testing of the network (i.e. network performance and linear regression).
- Retrain the network until a satisfactory small Mean Square Error (MSE) between the network outputs and targets is obtained.

Since, the size of the training set has a great influence on the generalization ability of the ANNs [24]. Three different configurations of calibration 4×10, 6×10 and 8×10, were designed to investigate the effect of sample size on the accuracy of the ANNs calibration algorithm to predict the in-plane stress components σ_{11}, σ_{12} and σ_{22}. In order to obtain reliable assessment on using the proposed ANNs for calibration of multi-element sensing rosettes, the sensors used in training and testing ANNs are the same sensors employed in the experimental sensitivity analysis.

In the 4×10 configuration, 40 calibration points obtained from the experimental testing of 4 different sensing chips were used to build ANN. While, in 6×10 configuration, 60 calibration points were collected from testing 6 different sensors under the same loading conditions of 4×10 configuration. Finally, using 8 different sensors, 80 calibration points were provided to construct ANN of 8×10 configuration.

In all three configurations, the sensing chip is attached to a PCB beam that is subjected to 10 different loads within a range from −7.5 to 7.5 N that produce 10 corresponding average stress values within a range from −40 to 40 MPa on the sensing chip surface.

C. Results and Discussions

In order to test the accuracy of the ANNS calibration algorithm in predicting the stresses, new experimental data set

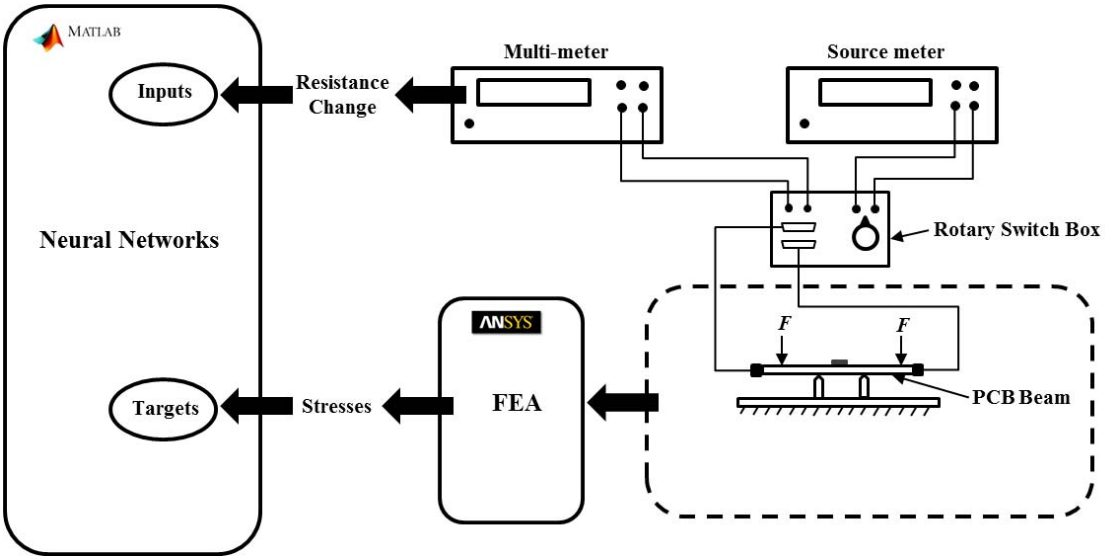

Fig. 12. Schematic of the testing setup.

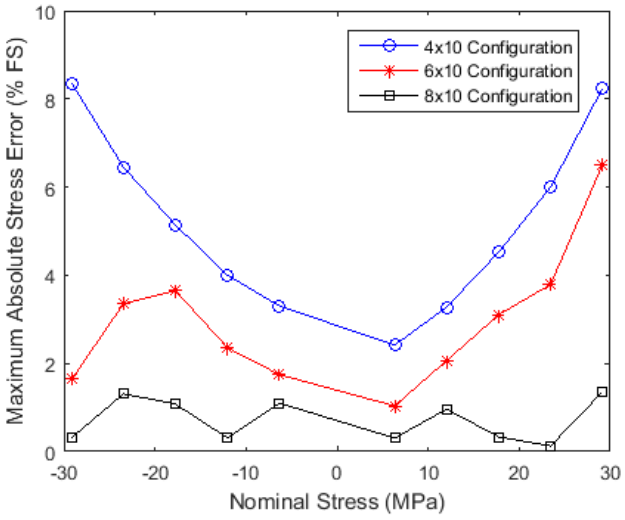

Fig. 13. Errors in measuring σ_{11} using neural network calibration algorithm.

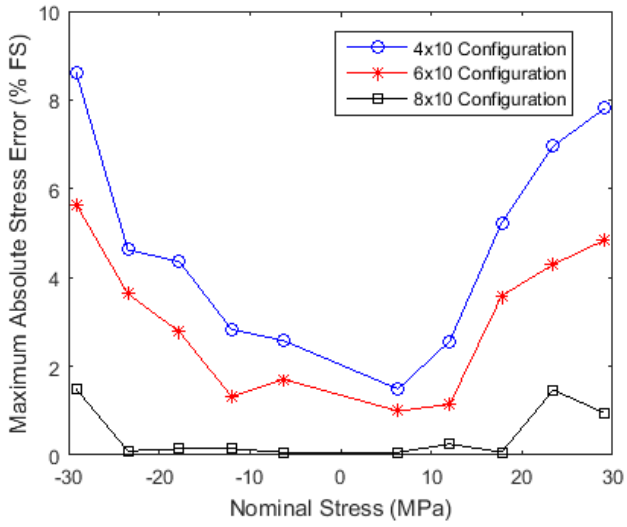

Fig. 14. Errors in measuring σ_{12} using neural network calibration algorithm.

were collected using new 5 randomly selected testing sensing chips. Each sensor of the 5 testing chips was subjected to 10 different loads within a range from −7.5 N to 7.5 N. The change in electrical resistance of each sensing element of the ten-element sensing rosette and the corresponding stresses, due to the applied load, were measured. Using these resistance change measurements as an input for the ANNs calibration algorithm, the predicted corresponding stresses, which are the ANNs output, can be calculated. Finally, these predicted stresses were compared with the actual stresses and the error was quantified.

Fig. 13 to Fig. 15 show the maximum absolute stress error between the predicted in-plane stress components σ_{11}, σ_{12} and σ_{22}, using the proposed ANNs calibration algorithm, and the in-plane stresses obtained from FEM for the same load. It can be found that the configuration 4×10 has the maximum error in extracting stresses compared to the other configurations, 6×10 and 8×10, since less calibration points were used in building ANN.

In 4×10 configuration, the maximum stress error can reach to 9% *FS*. It can also be clearly seen that increasing the sample size improves the accuracy of the constructed ANNs. As in 8×10 configuration, the maximum absolute stress error dropped to 1.5% *FS* while extracting the in-plane stress components σ_{11}, σ_{12} and σ_{22} using the proposed ANNs calibration algorithm. Our results also show that σ_{12} can be predicted with very high accuracy, unlike σ_{11} and σ_{22}. As shown in Fig. 14, for stress range from −20 to 20 MPa, the maximum error in σ_{12} doesn't exceed 0.25% *FS*. This can be attributed to using less input variables, while constructing the ANN of σ_{12}, than what were used in the ANNs of both σ_{11} and σ_{22}. As in ANN of σ_{12}, only 4 signals from piezoresistors R_2,R_4,R_6 andR_8 were used as inputs for ANN. Whereas in ANNs of σ_{11} and σ_{22}, 6 signals

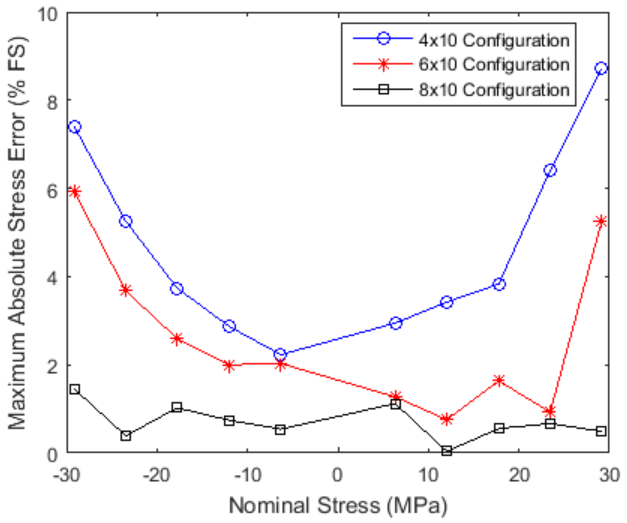

Fig. 15. Errors in measuring σ_{22} using neural network calibration algorithm.

from piezoresistors R_1,R_3,R_5,R_7, R_9 and R_{10}, were the inputs.

V. Conclusion

Numerical and Experimental sensitivity analyses have been carried out to study the effect of the variation in the PR coefficients' values on the accuracy of 3D piezoresistive stress sensor. This study showed that uncertainty of about 2.5% in the PR coefficients' values may result in large errors of 70% or more while monitoring the in-plane stresses on the sensing rosette. It has also been noticed that σ_{12} is less sensitive to the uncertainties in the PR coefficients thanσ_{11} and σ_{22}. A smart high accuracy calibration algorithm for 3D piezoresistive stress sensors is presented in this work.

A program was developed on MATLAB which incorporates the Neural Network Fitting Toolbox to build an ANNs that is capable of predicting the stresses generated on the sensing chip surface. Three different configurations of calibration were designed to test the generalization abilities of the ANNs in capturing the in-plane stress components exerted on the sensor's surface. The sensors used in training and testing ANNs are the same sensors employed in the experimental sensitivity analysis. The experimental results showed that the proposed algorithm can successfully extract the stresses with high accuracy of 1.5% *FS* despite the presence of the micro-fabrication non-uniformity. A minimum error was obtained when using 8×10 configuration, since larger calibration points were used to build the neural network compared to the other configurations.

Acknowledgment

The authors would like to thank the Canadian Microsystems Corporation and the Natural Sciences and Engineering Research Council of Canada for their support.

References

[1] A. A. Barlian, W. Park, J. R. M. Jr., A. J. Rastegar, B. L. Pruitt, and M. Engineering, "Review: Semiconductor piezoresistance for microsystems," *Proc. IEEE*, vol. 97, no. 3, pp. 513–552, Mar. 2009.

[2] D. A. Bittle, J. C. Suhling, R. E. Beaty, R. C. Jaeger, and R. W. Johnson, "Piezoresistive stress sensors for structural analysis of electronic packages," *J. Electron. Packag.*, vol. 113, no. 3, pp. 203–215, 1991.

[3] J. C. Suhling and R. C. Jaeger, "Silicon piezoresistive stress sensors and their application in electronic packaging," *IEEE Sensors J.*, vol. 1, no. 1, pp. 14–30, Jun. 2001.

[4] H. H. Gharib and W. A. Moussa, "On the feasibility of a new approach for developing a piezoresistive 3D stress sensing rosette," *IEEE Sensors J.*, vol. 11, no. 9, pp. 1861–1871, Sep. 2011.

[5] H. H. Gharib and W. A. Moussa, "A single-polarity piezoresistive three-dimensional stress-sensing rosette," *J. Microelectromech. Syst.*, vol. 20, no. 3, pp. 555–557, 2011.

[6] C. Chun-Hyung, J. C. Richard, and J. C. Suhling, "The effect of the transverse sensitivity on measurement of the piezoresistive coefficients of silicon," *Jpn. J. Appl. Phys.*, vol. 47, no. 5, pp. 3647–3656, 2008.

[7] R. C. Jaeger, C.-H. Cho, S. Hussain, and J. C. Suhling, "Impact of piezoresistive coefficient uncertainity on stress measurement using silicon multi-resistor sensor rosettes," in *Proc. IMECE*, 2008, pp. 1–12.

[8] S. Hussain, R. C. Jaeger, J. C. Suhling, J. C. Roberts, M. A. Motalab, and C. H. Cho, "Error analysis for piezoresistive stress sensors used in flip chip packaging," in *Proc. 12th IEEE Intersoc. Conf. Therm. Thermomech. Phenom. Electron. Syst. ITherm*, Jun. 2010, pp. 1–12.

[9] C. H. Cho, R. C. Jaeger, and J. C. Suhling, "Characterization of the temperature dependence of the piezoresistive coefficients of silicon from—150°C to +125°C," *IEEE Sensors J.*, vol. 8, no. 8, pp. 1455–1468, Aug. 2008.

[10] J. Scott and E. T. Enikov, "Novel temperature compensation technique for force-sensing piezoresistive devices," *J. Micromech. Microeng.*, vol. 21, no. 11, p. 115017, 2011.

[11] M. Aryafar, M. Hamedi, and M. M. Ganjeh, "A novel temperature compensated piezoresistive pressure sensor," *Measurement*, vol. 63, pp. 25–29, Mar. 2015.

[12] H. I. Kuo, J. Guo, and W. H. Ko, "High performance piezoresistive micro strain sensors," in *Proc. 2nd IEEE Int. Conf. Nano/Micro Eng. Molecular Syst. (NEMS)*, Jan. 2007, pp. 1052–1055.

[13] E. Perraud, "Theoretical model of performance of a silicon piezoresistive pressure sensor," *Sens. Actuators A Phys.*, vol. 57, no. 3, pp. 245–252, Dec. 1996.

[14] G. Zhou, Y. Zhao, F. Guo, and W. Xu, "A smart high accuracy silicon piezoresistive pressure sensor temperature compensation system," *Sensors (Switzerland)*, vol. 14, no. 7, pp. 12174–12190, 2014.

[15] D. Sonowal and M. Bhuyan, "Multi channel sensor linearization in field programmable gate array for real time applications," *Sensors Transducers*, vol. 191, no. 8, pp. 135–151, 2015.

[16] J. C. Patra, G. Chakraborty, and P. K. Meher, "Neural-network-based robust linearization and compensation technique for sensors under nonlinear environmental influences," *IEEE Trans. Circuits Syst. I, Reg. Papers*, vol. 55, no. 5, pp. 1316–1327, Jun. 2008.

[17] H. Erdem, "Implementation of software-based sensor linearization algorithms on low-cost microcontrollers," *ISA Trans.*, vol. 49, no. 4, pp. 552–558, Oct. 2010.

[18] N. J. Medrano-Marques and Martin-del-Brio, "A general method for sensor linearization based on neural networks," in *Proc. IEEE Int. Symp. Circuits Syst. Emerging Technol. 21st Century*, vol. 2, May 2000, pp. 497–500.

[19] N. J. Medrano-Marques and B. Martin-del-Brio, "Sensor linearization with neural networks," *IEEE Trans. Ind. Electron.*, vol. 48, no. 6, pp. 1288–1290, Dec. 2001.

[20] S. A. Khan, D. T. Shahani, and A. K. Agarwala, "Sensor calibration and compensation using artificial neural network," *ISA Trans.*, vol. 42, no. 3, pp. 337–352, Jul. 2003.

[21] H. H. Gharib and W. A. Moussa, "Microfabrication and calibration of a single-polarity piezoresistive three-dimensional stress sensing chip," *J. Micromech. Microeng.*, vol. 23, no. 3, p. 35019, 2013.

[22] A. A. Balbola, M. O. Kayed, and W. A. Moussa, "Studying the influence of n-type strained (111) silicon on the piezoresistive coefficients," *IEEE Sens. J.*, vol. 17, no. 2, pp. 302–310, 2016.

[23] A. G. Nagy, "Radial etch rate nonuniformity in reactive ion etching," *J. Electrochem. Soc.*, vol. 131, no. 8, p. 1871, 1984.

[24] E. L. Richards, "Generalization in neural networks: Experiments in speech recognition," Dept. Comput. Sci., Univ. Colorado, Boulder, CO, USA, Tech. Rep. CU-CS-538-91, 1991.

Mohammed O. Kayed received the B.Sc. and M.Sc. degrees from Cairo University, Egypt, in 2007 and 2011, respectively. He is currently pursuing the Ph.D. degree with the Department of Mechanical Engineering, University of Alberta, Canada.

From 2008 to 2011, he was a Research and Teaching Assistant with the Department of Mechanical Design and Production, Faculty of Engineering, Cairo University, where he was promoted to Lecturer Assistant, in 2011.

His research interests include MEMS, structural health monitoring, mechanical vibrations, and automatic control and robotics.

Amr A. Balbola received the B.Sc. and M.Sc. degrees from Cairo University, Egypt, in 2008 and 2013, respectively. He is currently pursuing the Ph.D. degree with the Department of Mechanical Engineering, University of Alberta.

From 2010, he was a Teaching and Research Assistant with Cairo University. His research interests include design, fabrication and testing of MEMS sensors, and strained silicon.

Walied A. Moussa received the B.Sc. and M.Sc. degrees from The American University in Cairo, in 1991 and 1993, respectively, and the Ph.D. degree from Carleton University, Ottawa, ON, Canada, in 2000.

He is currently a Professor with the University of Alberta, with co-appointment to the Mechanical Engineering, Biomedical Engineering, and the Department of Surgery. He has published more than 100 articles in his research fields. His current research interests include MEMS and NEMS research and development in the biomedical, aerospace, mechanical, and environmental fields. His research work involves both experimental and numerical approaches to this field.

Dr. Moussa has chaired the International Conference on MEMS, NEMS, and Smart Systems (ICMENS) from 2003 to 2006 and is on the editorial board of a number of related journals.